buildings

MDPI

Article

Structured Classification Feature-Guided FPFH-Based Coarse Registration Method for Precast T-Girders

Zijing Cen [1], Yuliang Cai [1,*], Jie Zhang [2] and Huan Zhang [2]

[1] Zhejiang Key Laboratory of Intelligent Construction and Operation & Maintenance for Deep-Sea Foundations, Ningbo University of Technology, Ningbo 315211, China
[2] Ningbo High Grade Highway Construction and Management Center, Ningbo 315199, China
* Correspondence: caiyuliang@nbut.edu.cn

Abstract

In precast girder yards, dense storage, limited scanning space, and mutual occlusion between girders make coarse registration of multi-station point clouds susceptible to noise, missing data, and insufficient overlap. To address these challenges, this study proposes an FPFH-based coarse registration method guided by structured classification features for precast prestressed concrete T-girders used in highway bridges. Based on the geometric characteristics of precast T-girders, engineering-oriented criteria are established to identify planar, linear, and corner features. Representative points from these features are then selected as FPFH descriptor centers. This introduces structural prior information into descriptor center selection while retaining the standard FPFH descriptor and SAC-IA coarse registration framework. Comparative experiments are conducted using 13 simulated Gaussian noise conditions and four local point cloud incompleteness conditions. The method is further validated using four scans of a single 30 m standard precast T-girder acquired at a precast girder yard. The results show that, compared with random-sampling FPFH, the proposed method reduces the coarse registration RMSE by 72.12% at a Gaussian noise level of 10 mm. Under local point cloud incompleteness ranging from 10% to 40%, the coarse registration RMSE is lower in all tested cases. At 40% incompleteness, the rotation errors about the three coordinate axes are reduced by more than 85% on average. The average runtime in the Gaussian noise simulations is reduced by 22.42%. For the field data, the average coarse registration RMSE and runtime are reduced by 62.42% and 28%, respectively. After ICP refinement, the average registration residual RMSE reaches 2.12 mm, representing an 80.97% reduction compared with random-sampling FPFH. These results indicate that the proposed method achieves favorable coarse registration performance under the tested conditions. It may provide a technical reference for multi-station point cloud merging and data preparation for subsequent geometric quality inspection of precast T-girders.

Keywords: precast T-girder; three-dimensional laser scanning; point cloud registration; FPFH feature descriptor; structured feature extraction

Check for updates

Academic Editor: Vipul Patel

Received: 30 September 2026
Revised: 19 October 2026
Accepted: 25 October 2026
Published: 27 October 2026

Copyright: © 2026 by the authors. Licensee MDPI, Basel, Switzerland. This article is an open access article distributed under the terms and conditions of the Creative Commons Attribution (CC BY) license.

1. Introduction

Precast T-girders are widely used in small- and medium-span prefabricated bridges. Their geometric dimensions and construction accuracy directly affect subsequent erection, component connections, and the in-service performance of bridges. Conventional quality inspection methods, such as manual measurement and visual inspection, are inefficient

and prone to limited accuracy, while the inspection data are difficult to preserve systematically. These limitations make them inadequate for quality control in large-scale batch production [1].

Three-dimensional (3D) laser scanning has emerged as a promising approach for geometric quality inspection of precast components because of its non-contact operation, high accuracy, and rapid full-field measurement capability. It can efficiently capture comprehensive three- dimensional geometric information of precast T-girders [2]. Owing to the large longitudinal dimensions and complex cross-sectional geometry of precast T-girders, a single scan station is generally insufficient to cover the entire girder surface. Multi-station scanning and point cloud registration are therefore required to reconstruct a relatively complete three-dimensional model. Accurate registration of multi-station point clouds is a prerequisite for point cloud stitching, subsequent geometric dimension inspection, and defect identification [3]. As the first stage of the registration process, coarse registration provides an initial pose for subsequent fine registration [4]. Its accuracy and robustness directly affect the convergence of the registration process and the final registration accuracy.

Fast Point Feature Histograms (FPFHs) [5] have been widely used for point cloud coarse registration because of their high computational efficiency and rotational invariance. However, most existing studies on FPFH have been validated using indoor scenes, industrial environments, or standard public datasets. These application scenarios generally feature relatively complete point clouds, limited occlusion, and low structural repetitiveness. In contrast, precast girder yards present much more complex scanning conditions. Dense girder storage and restricted scanning space can easily lead to local point cloud incompleteness and insufficient overlap between adjacent scans. In addition, the regular and repetitive geometry of precast components increases the similarity of local geometric features. Measurement noise of varying levels may also be introduced by equipment vibration and environmental disturbances during field data acquisition. These factors reduce the stability of local geometric feature representation in random-sampling FPFH-based coarse registration and consequently increase the uncertainty of feature matching [6,7].

To improve the robustness of FPFH descriptors in complex environments, Jia Zhenghua et al. [8] introduced dynamic downsampling to adaptively adjust the sampling density. Wang Yang et al. [9] enhanced the discriminative capability of local geometric features through multi-scale feature fusion. Jing Y. et al. [10] incorporated multimodal features, including intensity information, providing a new approach to improving the environmental adaptability of feature descriptors. However, these studies mainly focus on optimizing the descriptor construction process, while comparatively less attention has been paid to the strategy used for feature point selection. Conventional random-sampling FPFH-based coarse registration generally constructs the feature point set through random sampling or generic keypoint detection. The extracted features are therefore only weakly associated with the structural characteristics of the component. Under complex scanning conditions, this process may introduce redundant features with limited geometric distinctiveness, thereby reducing matching stability and computational efficiency.

In addition to improvements in feature descriptor construction, feature point selection is another important factor affecting point cloud registration performance. Existing studies have mainly focused on voxel-based sampling, local geometric information, and structural saliency. Zhao et al. [11] used voxel downsampling to select FPFH feature points. Su et al. [12] combined Intrinsic Shape Signatures (ISSs) with FPFH for point cloud registration. Yang et al. [13] employed 3D-SIFT to select feature points and improve registration efficiency. Regarding the use of local geometric information, Yang et al. [14] detected 3D keypoints based on structural saliency. Li et al. [15] combined principal directions with local voxel

structures to construct registration features. Slimani et al. [16] integrated local geometric attributes with learning-based feature descriptors to improve point cloud matching under challenging conditions.

For engineering components and challenging scanning environments, researchers have further incorporated structure-specific information to assist point cloud registration. Liu et al. [17] constructed feature descriptors using axial features of engine pipelines. Shan et al. [18] employed linear structural features for multi-view point cloud registration. Chen et al. [19] used contour turning features to improve the spatial localization of components with weak geometric features. In addition, Zhao et al. [20] used local region matching to guide the establishment of point correspondences. Gao et al. [21] jointly optimized keypoint detection and feature description. Guo et al. [22] utilized overlapping region information to improve feature matching. Xu et al. [23] combined structural and semantic information to improve point cloud registration performance.

Beyond these studies, methods based on component contours, local geometric features, and multi-station registration constraints have also been applied to point cloud registration for buildings and bridges [24–27]. To further clarify the technical characteristics of these methods, Table 1 compares representative studies in terms of feature selection strategies, registration frameworks, and validation objects.

Table 1. Comparison of representative point cloud feature selection and registration methods.

Reference	Feature Selection and Description	Registration Framework	Validation Data and Conditions	Main Difference from This Study
Zhao et al. [11] (2024)	Voxel-downsampled points as FPFH descriptor centers	RANSAC + ICP	Public point cloud datasets and measured stone point clouds	Focuses on voxel-based sampling and feature point selection
Yang et al. [13] (2025)	Feature points detected using normal thresholds and 3D-SIFT, followed by FPFH description	SAC-IA + ICP	Public point cloud datasets and measured data	Selects descriptor centers based on local geometric features
Yang et al. [14] (2025)	Keypoint detection based on structural saliency and local spatial geometry	Keypoint detection	Five keypoint detection benchmark datasets covering noise, point density, and geometric variations	Focuses on general keypoint detection based on structural saliency
Liu et al. [17] (2024)	PL-PPF descriptor constructed from pipeline axes and structural lines	Feature matching and SVD-based pose estimation	Aircraft engine pipelines under occlusion and missing-data conditions	Develops a specialized descriptor using pipeline structural priors
Chen et al. [19] (2025)	CIF descriptor constructed from contour turning features	Feature-based coarse registration + PSW-ICP	Aircraft skin inspection openings and their mating frames	Uses contour-based feature description and fine registration

Table 1. *Cont.*

Reference	Feature Selection and Description	Registration Framework	Validation Data and Conditions	Main Difference from This Study
Xiong et al. [26] (2024)	Registration organized using bridge templates, overlap relationships, and scan positions	Template-guided hierarchical multi-view registration	Measured point clouds of suspension and continuous rigid-frame bridges	Focuses on multi-station point cloud organization and global registration
This study	Planar, linear, and corner features extracted from T-girder geometry as FPFH descriptor centers	Standard FPFH + SAC-IA, followed by ICP for field data	Simulated point clouds of a standard 30 m T-girder and four scans of a single field T-girder	Selects FPFH descriptor centers using T-girder structural priors

As shown in Table 1, existing methods differ in their approaches to feature selection and the use of structural information. For precast T-girders, the main planar surfaces and structural boundaries exhibit regular and repetitive geometric patterns. In contrast, girder ends, flange–web junctions, and diaphragms have distinct structural features. Therefore, establishing descriptor center selection criteria based on the geometric characteristics of precast T-girders has practical value for engineering research.

To address these issues, this study proposes an FPFH-based coarse registration method guided by structured classification features for precast T-girders in complex girder-yard environments. The method utilizes the regular and well-defined geometric characteristics of industrially manufactured T-girders. First, a structured feature system consisting of planar, linear, and corner features is developed based on the geometry of precast T-girders. Identification criteria are defined for each feature category, and the features are extracted using established point cloud processing methods. Second, representative points from the three feature categories are combined into a unified feature point set and used as FPFH descriptor centers instead of randomly sampled points. The standard FPFH descriptor is retained, and coarse registration is performed using the Sample Consensus Initial Alignment (SAC-IA) algorithm. Finally, simulation experiments under different noise levels and point cloud incompleteness ratios are conducted to examine changes in coarse registration residuals, pose errors, and runtime. The method is further evaluated using field point clouds acquired from four scan stations for a single 30 m precast T-girder to assess its registration performance and practical feasibility.

The main contribution of this study is to use the geometric characteristics of precast T-girders to select FPFH descriptor centers. This establishes an engineering-oriented structured feature selection method while retaining the standard FPFH descriptor and SAC-IA registration framework.

2. Point Cloud Registration and Noise Characterization

2.1. Rigid Point Cloud Registration

Rigid registration aligns point clouds solely through spatial pose transformation without altering the geometric shape of the component. It has been widely applied in engineering scenarios such as bridge component inspection and multi-station laser-scanning point cloud registration. Because precast T-girders can be treated as rigid bodies, the transformation between point clouds acquired from different scan stations involves only rotation and translation, without scaling or deformation. Therefore, a rigid registration model is adopted in this study. The key objective is to determine the optimal rotation

matrix and translation vector so that the source point cloud is best aligned with the target point cloud in the least-squares sense. At present, singular value decomposition (SVD) is one of the most widely used methods for solving this problem because of its numerical stability and reliable accuracy [28].

2.2. Fast Point Feature Histograms (FPFHs)

The FPFH descriptor is a general-purpose local feature descriptor for point clouds [5]. It characterizes local point cloud geometry using angular relationships between neighboring points, as illustrated in Figure 1.

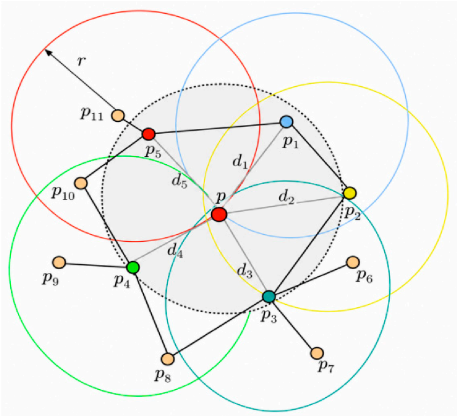


Figure 1. The influence region diagram for a Fast Point Feature Histogram. The query point (red) and its direct neighbors (multicolored), each associated with a local neighborhood of radius r, are illustrated, with pairwise distances d_1–d_5 between the query point and its neighbors annotated.

The computation of the FPFH descriptor consists of two main steps:

1. SPFH computation: For the query point p, the relative geometric relationship with each first-order neighboring point p_k is encoded as three angular features $(\alpha, \varphi, \theta)$. These angular features are then binned into a histogram to construct the Simplified Point Feature Histogram (SPFH) descriptor for the query point p.

(2) Weighted neighborhood aggregation: The SPFH descriptors of the first-order neighboring points are aggregated using inverse distance weighting to incorporate information from their local neighborhoods, as illustrated in Figure 1. The weight assigned to each neighboring point is determined by its Euclidean distance d_k from the query point p. The FPFH descriptor of the query point p is then computed as follows:

$$FPFH(p) = SPFH(p) + \frac{1}{k}\sum_{k=1}^{w} \frac{1}{wk} \cdot SPFH(pk)$$

FPFH characterizes local geometry by statistically describing geometric relationships within the neighborhood of each feature point. Its registration performance depends not only on how the descriptor is constructed, but also on the stability of the descriptor centers and their local neighborhoods. Noise, repetitive geometry, and point cloud incompleteness can all reduce the discriminative capability of local features. In addition, involving a large number of poorly discriminative feature points in the matching process increases computational cost. Conventional FPFH-based coarse registration generally determines descriptor centers through random sampling or uniform downsampling, with limited use of component-level structural information. Therefore, while retaining the original mathematical formulation of FPFH, this study focuses on the engineering-oriented selection of descriptor centers to strengthen the association between the selected feature points and the primary structural characteristics of precast T-girders.

2.3. Point Cloud Interference Characteristics in Precast Girder Yards

As an industrial site for the batch production of precast components, a precast girder yard is characterized by complex scanning conditions, including densely arranged girders, restricted scanning space, and severe mutual occlusion between adjacent components, as shown in Figure 2.



Figure 2. Precast T-girder storage yard.

Under such conditions, point clouds acquired by 3D laser scanning are susceptible to multiple sources of interference, including instrument measurement errors, environmental disturbances, and occlusion. These factors can degrade point cloud quality and distort local geometric information. Based on their sources and effects on feature stability, the main influencing factors can be classified into the following three categories:

(1) **Environmental noise:** This type of noise mainly arises from the intrinsic systematic errors of laser scanners and signal attenuation during long-range scanning [29]. For general terrestrial laser scanners, measurement noise within a range of 0–100 m is typically about 0.5–10 mm. In complex field environments, structured point-cloud artifacts may also occur, further interfering with the registration process.

(2) **Initial scan-station pose error:** Point clouds acquired from multiple scan stations are typically expressed in their respective local coordinate systems and require rotation and translation transformations for spatial alignment. Errors in the initial transformation parameters can lead to inaccurate estimates of the relative poses between scans [30]. Unlike measurement noise, this type of error primarily affects the overall relative position and orientation of the point clouds.

(3) **Local occlusion and point cloud incompleteness:** These effects are mainly caused by surface occlusion, contamination, variations in reflectivity, and surface roughness. They typically result in local data gaps, reduced point density, and incomplete geometric information. Such factors can introduce local deviations of approximately 5–15 mm. Among them, the loss of geometric information caused by occlusion has the most pronounced effect on registration stability [31].

The factors described above affect point cloud registration in different ways. Measurement noise and local point cloud incompleteness mainly affect the integrity of geometric information and the reliability of feature description. In contrast, initial scan-station pose errors primarily affect the relative spatial relationships between point clouds acquired

from different scan stations. This study focuses on structured feature selection and coarse registration performance under noise and point cloud incompleteness conditions, aiming to improve the adaptability of precast T-girder point cloud registration in challenging scanning environments.

3. Structured Classification Feature-Guided FPFH-Based Coarse Registration Method

3.1. Structured Feature Definition and Identification Criteria for Precast T-Girders

A precast T-girder is typically composed of regular structural components, such as the flange slab, web, and diaphragms, as shown in Figure 3. From a geometric perspective, the girder surface contains large-scale, approximately planar regions, structural boundaries formed at the intersections of adjacent planes, and local geometric transitions at contour or component intersections. These geometric characteristics correspond to three feature types: planar, linear, and corner features. Compared with randomly sampled points, these locations have a clearer correspondence with the primary structural components of the T-girder. This makes it easier to incorporate engineering prior knowledge into point cloud processing and to interpret the structural origin of the extracted features. Therefore, planar, linear, and corner features are adopted as the basic components of the structured classification feature system in this study.

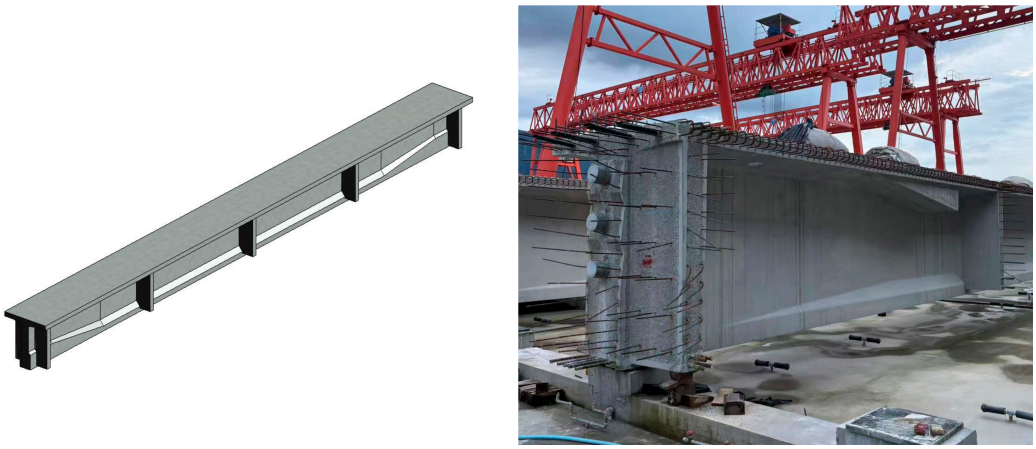


Figure 3. Structural schematic of a precast T-girder.

To ensure that the above structural features accurately represent the primary geometry of the girder and improve the stability and discriminative capability of subsequent FPFH descriptors, classification criteria are established from three aspects: structural location, extraction method, and geometric constraints. The definitions and identification criteria for the three types of structured features are summarized in Table 2.

Table 2 translates the typical geometric characteristics of precast T-girders into specific criteria for feature selection. These criteria establish clear relationships between the extracted feature points and the main structural components of the girders. However, this feature system relies on the relatively regular geometry of precast T-girders. For other girder types or irregular precast components with substantially different cross-sectional shapes or component arrangements, the identification criteria need to be adjusted according to their geometric characteristics. The specific parameter settings are provided in Section 4.1.

This study primarily evaluates the effect of structured feature selection on FPFH coarse registration performance under fixed feature identification thresholds. The relevant parameters remain unchanged across all comparative experiments, and no separate threshold sensitivity analysis is conducted.

Table 2. Definition and identification criteria of structured features for precast T-girders.

Feature Type	Feature Location	Feature Extraction Method	Geometric Constraints
Planar Feature	Continuous planar regions, such as flange top surfaces and web side surfaces	Normal vector clustering and RANSAC plane fitting	① Point-to-plane distance below threshold ε_p ② Normal vector consistency requirement satisfied ③ Planar area greater than threshold $A_{\min}$
Linear Feature	Plane intersections and component boundaries	Boundary point extraction and Hough transform-based line detection	① Continuous point cloud distribution along the principal direction ② Line segment length greater than threshold $L_{\min}$ ③ Line fitting residual below threshold ε_l
Corner Feature	Corner regions and structural intersections	α-shape boundary reconstruction and feature intersection calculation	① Orthogonality deviation between adjacent plane normals below threshold θ_{max} ② Located at contour turning points or structural intersections ③ Duplicate corners removed through spatial clustering

3.2. Structured Classification Feature Extraction

To make full use of the structural prior information of precast T-girders, this study adopts a hierarchical feature extraction strategy following the sequence of planar, linear, and corner features. First, the primary planar features of the girder are extracted. Structural linear features are then identified based on planar boundaries and their spatial relationships. Finally, corner features are determined according to the geometric relationships between planar contours and structural lines. All feature types are extracted using established point cloud processing methods and organized according to the geometric hierarchy of precast T-girders. The overall workflow is illustrated in Figure 4.

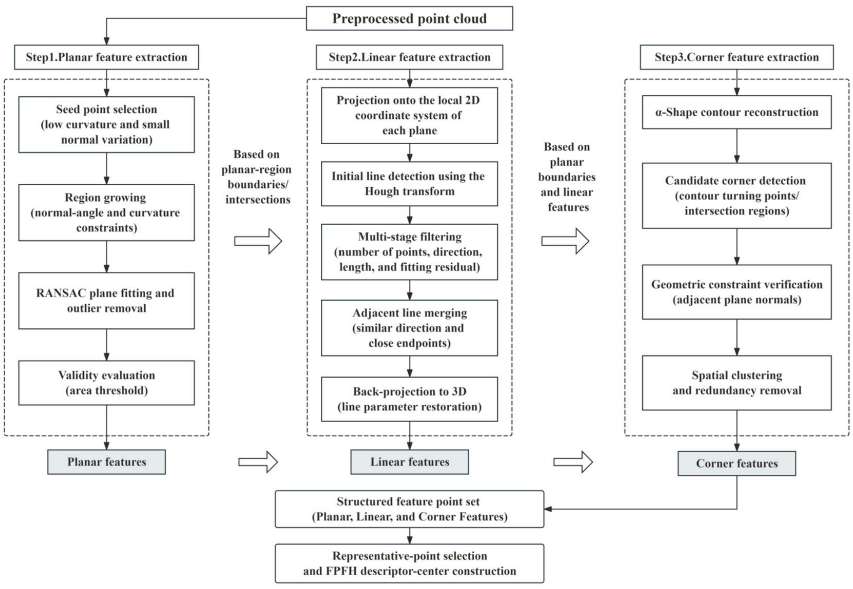


Figure 4. Structured Classification Feature Extraction and Descriptor Center Construction Workflow.

(1) Planar Feature Extraction

The main planar surfaces of the T-girder are identified by combining region growing with RANSAC plane fitting. First, local neighborhoods are constructed using K-nearest neighbor search. Region growing is then performed based on normal-angle and local curvature constraints to identify candidate planar regions. Next, RANSAC plane fitting is applied to each candidate region. Inliers are determined using a point-to-plane distance threshold, and candidate planes with insufficient supporting points are removed. Finally, the main planar features are selected based on a minimum planar area requirement.

(2) Linear Feature Extraction

Based on the identified planar regions, the corresponding point clouds are projected onto local 2D coordinate systems. The Hough transform is then applied to detect candidate lines. Valid line segments are selected based on the number of supporting points, direction, segment length, and fitting residual. Next, adjacent line segments satisfying the spatial distance and directional consistency constraints are merged. Finally, the merged line segments are transformed back into 3D space to obtain linear features representing structural intersections and component boundaries.

(3) Corner Feature Extraction

Corner feature extraction is based on the spatial relationships between planar boundaries and structural lines. First, the α-shape algorithm is used to reconstruct the outer boundaries of planar regions. Candidate corners are then identified from contour turning points and intersections of structural lines. Next, candidate corners at structural intersections are evaluated based on the orthogonality of adjacent plane normals. Only those satisfying the geometric constraints are retained. Finally, spatial distance clustering is applied to merge and remove redundant candidate corners. The final corner position is determined by averaging the coordinates of the candidate points within each cluster.

3.3. Structured Classification Feature-Guided FPFH Descriptor Center Selection

Descriptor centers for FPFH-based coarse registration can be selected through random sampling, uniform sampling, or keypoint detection. For precast T-girders with regular geometries and repetitive local structures, random sampling cannot reliably ensure that the selected points cover structural boundaries, changes in orientation, and geometric transitions. This limitation may affect the stability of feature description and matching, particularly under noise and local point cloud incompleteness.

To investigate the influence of structural priors on FPFH coarse registration performance, random-sampling FPFH, which does not rely on structural priors, is selected as the baseline method. Both methods use the same FPFH descriptor and SAC-IA coarse registration framework. After planar, linear, and corner features are identified through the preceding steps, one representative point is selected from each feature. These points form a unified structured feature point set and serve as FPFH descriptor centers. This establishes direct relationships between the descriptor centers and the main planar surfaces, structural boundaries, and geometric transitions of the T-girder. Both methods use the same parameters for normal estimation and FPFH neighborhood search. The SPFH computation and weighted aggregation procedures also remain unchanged. The specific parameters and point cloud preprocessing settings are provided in Section 4.1.

After FPFH feature description, candidate correspondences are established through matching in feature space. SAC-IA is then used to estimate the initial rigid transformation between the source and target point clouds. The three categories of structured features are used jointly, and their extraction follows a hierarchical process with dependencies between successive stages. No separate matching is performed for individual feature categories, and

no category-specific weights or additional geometric constraints are introduced. Therefore, this study primarily evaluates the overall registration performance of structured feature selection within the standard FPFH framework. No further conclusions are drawn regarding the independent contribution of each feature category or the relative performance of other registration methods.

4. Experimental Results and Analysis

To evaluate the performance of the structured feature selection strategy under different point cloud conditions, this study conducts both simulation and field experiments. The simulation experiments mainly examine the effects of noise and point cloud incompleteness on coarse registration residuals, pose errors, and runtime. The field experiments evaluate the practical performance of the proposed method through multi-station point cloud registration. Both methods use the same FPFH descriptor and SAC-IA coarse registration framework. ICP is also applied consistently to both methods for fine registration in the field experiments.

4.1. Experimental Setup

The experiments were conducted in a Python 3.10 environment using Open3D 0.19.0 for algorithm implementation and visualization. All experiments were performed on a workstation equipped with an Intel Xeon Gold 6238 CPU @ 2.10 GHz (22 cores and 44 logical processors), an NVIDIA GeForce GPU, and a 64-bit Windows 10 operating system.

Planar feature extraction employs K-nearest neighbor region growing with a neighborhood size of 20 points, a normal-angle tolerance of 10°, and a local curvature threshold of 0.005. For RANSAC plane fitting, the inlier distance threshold ε_p is set to 0.010 m, the minimum number of supporting points is 500, and the maximum number of iterations is 3000. The minimum planar area Amin is set to 0.02 m^2. No separate plane merging operation is performed.

Linear feature extraction uses the 2D Hough transform to detect candidate lines. The distance and angular resolutions are set to 0.005 m and 1°, respectively. The directional tolerance is 5°, and the minimum number of supporting points is 80. The minimum length of candidate line segments is set to 0.05 m, with a fitting residual threshold of 0.008 m. Adjacent line segments with a spatial distance of less than 0.01 m and an angular difference of less than 5° are merged according to the predefined merging criteria.

Corner feature extraction uses the α-shape algorithm to reconstruct planar boundaries. The α parameter is set to 0.03 m, and no separate contour simplification is performed. For candidate corners at structural intersections, geometric validity is evaluated based on the angle between adjacent plane normals. The maximum deviation from orthogonality is set to 15°, corresponding to an allowable angle range of 75–105°. The spatial clustering tolerance for candidate corners is set to 0.015 m. Candidate corners satisfying the distance criterion are grouped into the same cluster, and the mean coordinates of the candidate points within each cluster are used to determine the final corner position.

FPFH feature description uses consistent neighborhood search parameters. The search radius for normal estimation is set to 0.05 m, with a maximum of 50 neighbors. The FPFH descriptor uses a support radius of 0.08 m and a maximum of 80 neighbors. Both methods use identical feature description parameters.

In the coarse registration stage, SAC-IA is used to estimate the initial rigid transformation. Four-point correspondences are sampled for each pose hypothesis. The maximum correspondence distance is set to 0.02 m, and the maximum number of iterations is 1000. The registration process terminates when the maximum number of iterations is reached or when the best transformation model remains unchanged for 200 consecutive iterations.

During registration, sample consensus verification is used to retain point correspondences that satisfy the distance constraint.

In the fine registration stage, the point-to-plane ICP algorithm is applied, using the rigid transformation obtained from SAC-IA as the initial estimate. The maximum correspondence distance is set to 0.015 m, and the maximum number of iterations is 100. According to the convergence criteria implemented in Open3D, the process terminates when the relative changes in both inlier RMSE and registration fitness between successive iterations fall below 10^{-6}, or when the maximum number of iterations is reached.

The above parameters remain unchanged across all experimental conditions, regardless of noise level or point cloud incompleteness ratio. The subsequent experiments mainly compare the registration performance of different descriptor center selection strategies under identical parameter settings.

4.2. Coarse Registration Experiments on Simulated Point Clouds

The simulated point clouds are generated from a BIM model of a standard 30 m precast T-girder. Approximately one million points are uniformly sampled from the triangular mesh surfaces of the model to construct a baseline point cloud, as shown in Figure 5. Both the source and target point clouds are generated from the same baseline point cloud. A predefined rigid transformation is applied to introduce an initial pose difference between them. Based on these point clouds, 13 Gaussian noise conditions and four local point cloud incompleteness conditions are established, resulting in 17 test conditions in total.

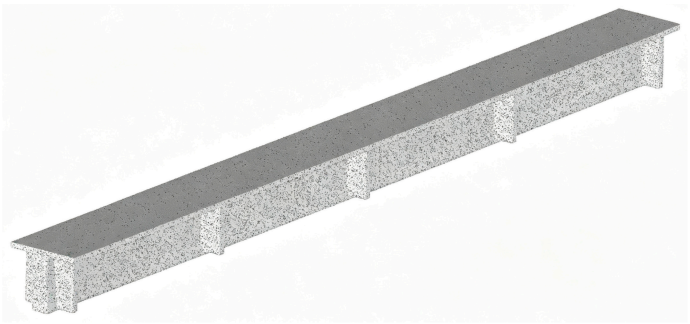


Figure 5. Simulated point cloud model of the precast T-girder.

Zero-mean Gaussian noise is applied independently to the X, Y, and Z coordinates of each point. The noise level is characterized by the standard deviation σ, ranging from 0.5 to 15 mm. The 15 mm high-noise condition is mainly used to evaluate feature identification and registration performance under strong perturbations. It does not represent the typical measurement error of conventional laser scanning instruments.

Local point cloud incompleteness conditions are generated by randomly selecting spatial regions and removing the points within them. The incompleteness ratios range from 10% to 40% to simulate the loss of geometric information caused by local occlusion. These ratios mainly reflect the overall reduction in point cloud data and do not directly indicate the extent of missing data in critical structural regions of the girder. The experiments separately examine the effects of noise and point cloud incompleteness on structured feature extraction and coarse registration results. Initial pose error is not treated as an independent experimental variable.

To reduce computational cost, the simulated point clouds are downsampled using a voxel filter with a voxel size of 0.02 m. The centroid of the points within each voxel is used as the representative point, reducing the number of points from approximately one million to fewer than 50,000. The preprocessing results are shown in Figure 6. Both methods use the same preprocessed point clouds and FPFH descriptor parameters, with SAC-IA applied

for coarse registration. This allows a comparison of the registration performance of two descriptor center selection strategies: random sampling and structured feature selection.

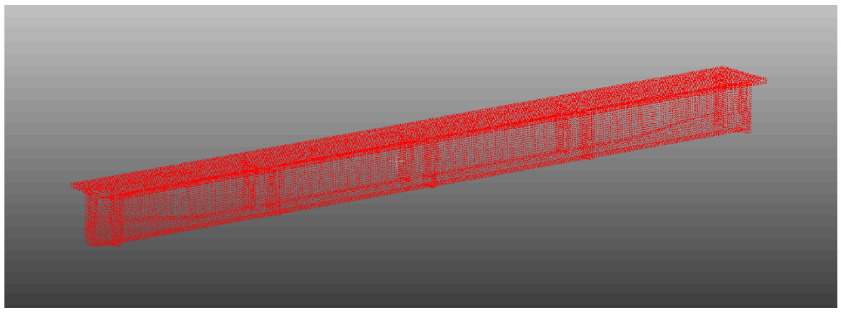


Figure 6. Preprocessing results of the simulated point clouds.

4.2.1. Structured Feature Extraction and Descriptor Center Statistics

The structured classification features are extracted from the simulated point clouds and visualized using color coding, as shown in Figure 7. Planar features are marked in red and cover the main structural surfaces of the T-girder. Linear features are shown in green and are mainly distributed along girder edges and structural intersection lines. Corner features are marked in blue and are concentrated at key locations where abrupt geometric changes occur in the T-girder.

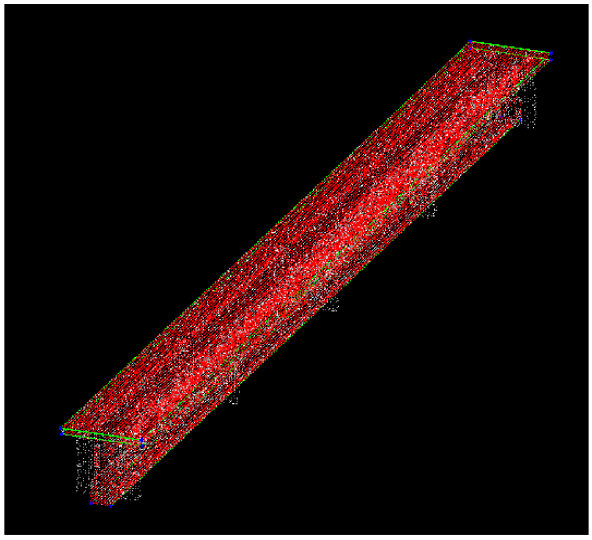


Figure 7. Structured classification feature extraction from the simulated precast T-girder point cloud.

The number of identified features under different experimental conditions is presented in Table 3. At noise levels ranging from 0.5 to 5.0 mm, the numbers of planar, linear, and corner features remain unchanged. When the noise level increases to 6.0 mm, some linear and corner features are no longer identified because they fail to meet the predefined selection criteria. At noise levels of 7.0 mm and above, the number of identified features decreases further, with mainly the major planar surfaces, principal structural edges, and key contour turning points retained.

In contrast, the numbers of all three feature categories remain unchanged under point cloud incompleteness ratios of 10–40%. This indicates that the tested incompleteness patterns do not reduce the number of identifiable structural features. However, unchanged feature counts do not necessarily mean that local geometric information remains unaffected. The effects of missing data on registration performance are further examined in the following experiments.

Table 3. Number of identified features by feature type under different experimental conditions.

Test Condition	Number of Planar Features	Number of Linear Features	Number of Corner Features
Original Point Cloud	5	10	12
Noise level: 0.5 mm	5	10	12
Noise level: 1.0 mm	5	10	12
Noise level: 1.5 mm	5	10	12
Noise level: 2.0 mm	5	10	12
Noise level: 2.5 mm	5	10	12
Noise level: 3.0 mm	5	10	12
Noise level: 5.0 mm	5	10	12
Noise level: 6.0 mm	5	8	10
Noise level: 7.0 mm	3	6	8
Noise level: 8.0 mm	3	6	8
Noise level: 9.0 mm	3	6	8
Noise level: 10.0 mm	3	6	8
Noise level: 15.0 mm	3	6	8
Point cloud incompleteness: 10%	5	10	12
Point cloud incompleteness: 20%	5	10	12
Point cloud incompleteness: 30%	5	10	12
Point cloud incompleteness: 40%	5	10	12

To compare the number of points used for feature description by the two methods, the FPFH descriptor center counts under different experimental conditions are summarized in Table 4. Structured-feature FPFH (S-FPFH) selects one representative point from each identified planar, linear, and corner feature as a descriptor center. In contrast, random-sampling FPFH (R-FPFH) selects descriptor centers through random sampling, and the number of sampled points is equal to the number of corner features identified under each experimental condition.

Table 4. Number of FPFH descriptor centers under different experimental conditions.

Test Condition	Number of R-FPFH Descriptor Centers	Number of S-FPFH Descriptor Centers
Original point cloud	12	27
Noise level: 0.5–5.0 mm	12	27
Noise level: 6.0 mm	10	23
Noise level: 7.0–15.0 mm	8	17
Point cloud incompleteness: 10–40%	12	27

As shown in Table 4, the number of descriptor centers used by both methods decreases as the noise level increases, but remains unchanged under the point cloud incompleteness conditions considered in this study. It should be noted that the two methods use different numbers of descriptor centers. Therefore, the subsequent registration results mainly reflect the overall performance of the two descriptor center selection strategies under the specified experimental settings.

4.2.2. Comparison of Registration Results

To quantitatively evaluate the coarse registration performance of different feature point selection strategies, this study uses the root mean square error (RMSE), rotation error, and translation error as evaluation metrics. RMSE measures the geometric alignment residual between the source and target point clouds after registration. Rotation error and translation error are used to evaluate the differences between the estimated rigid transformation and

the ground-truth transformation predefined in the simulation. The evaluation metrics are calculated as follows:

The RMSE is calculated using the nearest-neighbor distances between the registered source point cloud and the target point cloud, as follows:

$$RMSE = \sqrt{\frac{1}{N}\sum_{i=1}^{N}\left\|\hat{\mathbf{R}}p_i + \hat{\mathbf{t}} - q_i\right\|^2} \quad (1)$$

where N is the number of valid point correspondences used for evaluation; p_i denotes the i-th point in the source point cloud; q_i denotes the corresponding point in the target point cloud for the transformed source point; and $\hat{\mathbf{R}}$ and $\hat{\mathbf{t}}$ represent the estimated rotation matrix and translation vector, respectively.

Rotation error measures the difference between the estimated rotation and the ground-truth rotation. The angular errors about the X, Y, and Z axes are expressed as follows:

$$e_{R,k} = \left|wrap(\hat{\theta}_k - \theta_k^*)\right| \quad (2)$$

where $e_{R,k}$ denotes the rotation error about the corresponding coordinate axis; $\hat{\theta}_k$ and θ_k^* represent the angular components obtained by decomposing the estimated and ground-truth rotation matrices, respectively, using the same Euler-angle convention; and *wrap* normalizes the angular difference to the range $[-\pi, \pi]$. The rotation error is expressed in radians (rad).

Translation error measures the difference between the estimated translation vector and the ground-truth translation vector. It is expressed as follows:

$$e_t = \|\hat{\mathbf{t}} - \mathbf{t}^*\|_2 \quad (3)$$

where e_t denotes the translation error; $\hat{\mathbf{t}}$ and $\mathbf{t}^*$ represent the estimated and ground-truth translation vectors, respectively. The unit is millimeters (mm).

For the noise and point cloud incompleteness conditions, coarse registration is performed using random-sampling FPFH (R-FPFH) and structured-feature FPFH (S-FPFH). Both methods use SAC-IA to estimate the initial transformation. Considering the randomness involved in random sampling and SAC-IA registration, each experimental condition is evaluated through 10 repeated runs. The registration metrics are reported as the average values of these 10 runs. Table 5 presents a comparison of the coarse registration residuals obtained by the two methods at different noise levels.

As shown in Table 5, both methods achieve relatively low coarse registration RMSE values at noise levels ranging from 0.5 to 5 mm, with only minor differences between them. When the noise level increases to 6–7 mm, the RMSE values of S-FPFH reach 29.7 mm and 34.3 mm, respectively, exceeding those of R-FPFH (26.8 mm and 26.2 mm). As indicated in Tables 3 and 4, some linear and corner features are no longer identified at these noise levels because they fail to meet the predefined identification criteria. Consequently, the number of structured descriptor centers decreases from 27 to 23 and then to 17. These changes in the feature point set may affect the local representation of key geometric structures and subsequent feature matching, leading to fluctuations in registration performance. This indicates that the proposed method depends, to some extent, on the stability of the preceding feature extraction process.

As the noise level increases further to 8–15 mm, the registration residuals of both methods increase, but the increase is more pronounced for R-FPFH. At noise levels of 10 mm and 15 mm, the RMSE values of R-FPFH reach 136.3 mm and 232.1 mm, respectively, compared with 38.0 mm and 76.3 mm for S-FPFH. These results indicate a relatively smaller

increase in registration residuals for S-FPFH. As shown in Table 4, although the number of structured descriptor centers remains at 17 within this noise range, the retained features are still associated with the main geometric structures of the girder. This may help preserve the structural distinctiveness of local feature descriptors. Overall, S-FPFH shows a relative advantage under the higher noise levels considered in this study. However, its registration performance remains affected by the stability of feature extraction. The RMSE trends of the two methods are shown in Figure 8.

Table 5. Comparison of coarse registration RMSE between the two methods under different noise levels.

Noise Level (mm)	R-FPFH Coarse Registration RMSE (mm)	S-FPFH Coarse Registration RMSE (mm)	RMSE Reduction (%)
0.5	4.4	4.4	0.00%
1.0	4.4	4.4	0.00%
1.5	4.5	4.5	0.00%
2.0	4.6	4.5	2.17%
2.5	4.5	4.5	0.00%
3.0	4.5	4.5	0.00%
5.0	6.2	5.8	6.45%
6.0	26.8	29.7	−10.82%
7.0	26.2	34.3	−30.92%
8.0	52.7	36.1	31.50%
9.0	91.5	37.2	59.34%
10.0	136.3	38.0	72.12%
15.0	232.1	76.3	67.13%

Note: The coarse registration results under each experimental condition are the average values of 10 repeated runs.

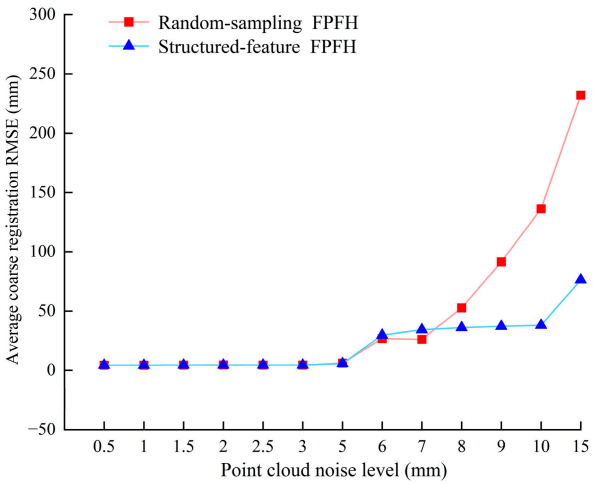


Figure 8. Variation in coarse registration RMSE with noise level for the two methods.

It should be noted that this study uses independent Gaussian perturbations to simulate measurement noise. The effects of scanning distance, incidence angle, and surface reflectivity on actual measurement errors are not considered. Therefore, the above results mainly reflect registration performance under the simulated noise conditions considered in this study.

In addition to noise, local point cloud incompleteness can also affect coarse registration results. To evaluate the performance of the two methods under different incompleteness ratios, their RMSE, rotation errors, and translation errors are further compared at point cloud incompleteness ratios ranging from 10% to 40%. The results are presented in Table 6.

Table 6. Comparison of coarse registration results between the two methods under different point cloud incompleteness levels.

Point Cloud Incompleteness (%)	RMSE (mm)		Rotation Error (Rad)						Translation Error (mm)	
			X		Y		Z			
	R-FPFH	S-FPFH	R-FPFH	S-FPFH	R-FPFH	S-FPFH	R-FPFH	S-FPFH	R-FPFH	S-FPFH
0 (Ref.)	0.0000	0.0000	0.0000	0.0000	0.0000	0.0000	0.0000	0.0000	0.0000	0.0000
10	4.4460	4.4020	0.0104	0.0008	0.0207	0.0016	0.0145	0.0011	0.5870	0.4720
20	5.4860	5.0690	0.0114	0.0007	0.0227	0.0013	0.0159	0.0009	0.8250	0.7210
30	6.7430	6.2510	0.0134	0.0058	0.0268	0.0106	0.0188	0.0081	2.3820	1.4850
40	7.7120	7.0800	0.0150	0.0021	0.0299	0.0044	0.0209	0.0029	2.2720	2.1050

Note: Ref. = Reference condition. X, Y, and Z denote the three coordinate axes of the simulated reference point cloud coordinate system. The corresponding rotation errors represent the differences between the angular components of the estimated and ground-truth rotations about each axis, expressed in radians (rad). Translation error is defined as the Euclidean distance between the estimated and ground-truth translation vectors, expressed in millimeters (mm). The coarse registration results under each experimental condition are the average values of 10 repeated runs.

As shown in Table 6, the coarse registration RMSE values of both methods generally increase as the point cloud incompleteness ratio increases. However, S-FPFH achieves lower registration residuals under all tested conditions. At a point cloud incompleteness ratio of 40%, the RMSE decreases from 7.712 mm for R-FPFH to 7.080 mm for S-FPFH. The rotation errors about the three coordinate axes are reduced by more than 85% on average, indicating a more pronounced improvement in rotation estimation. The variations in rotation errors at different point cloud incompleteness ratios are shown in Figure 9.

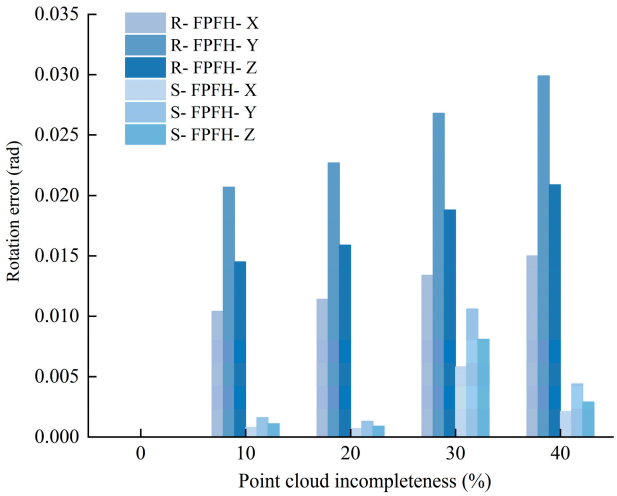


Figure 9. Comparison of rotation errors along the x-, y-, and z-axes under different levels of point cloud incompleteness.

Based on the preceding feature count statistics, the numbers of identified planar, linear, and corner features remain unchanged at point cloud incompleteness ratios of 10–40%. This indicates that the simulated local incompleteness does not reduce the number of major structural features. This finding may partly explain the favorable registration performance of S-FPFH under these conditions. It should be noted that the point cloud incompleteness ratio mainly reflects the overall reduction in the number of points. It does not directly represent the extent of missing data in critical regions, such as the outer boundaries of the flange, the flange-web intersections, and the diaphragm edges.

4.2.3. Runtime Comparison

The average coarse registration runtimes of the two methods at different noise levels are presented in Table 7, and the corresponding trends are shown in Figure 10.

Table 7. Comparison of average runtime between the two methods under different noise levels.

Noise Level (mm)	Average Runtime (s)		Runtime Reduction (%)
	R-FPFH Runtime (s)	S-FPFH Runtime (s)	
0.5	22.3198	19.9025	10.83%
1.0	24.0027	20.0256	16.57%
1.5	24.6281	18.7681	23.79%
2.0	24.3653	21.1344	13.26%
2.5	24.5138	17.9163	26.91%
3.0	36.7963	28.6035	22.27%
5.0	68.5747	52.2249	23.84%
6.0	75.1733	57.0975	24.05%
7.0	72.8471	55.1104	24.35%
8.0	69.7681	52.6613	24.52%
9.0	67.9363	49.7502	26.77%
10.0	64.6658	48.6057	24.84%
15.0	62.1288	43.7919	29.51%

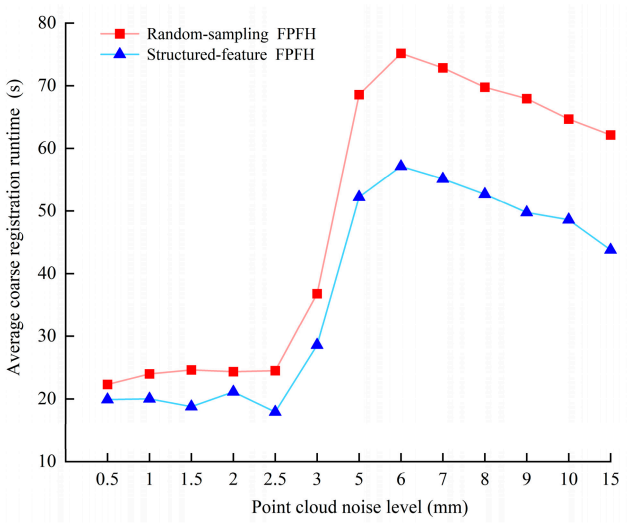


Figure 10. Variation in coarse registration runtime with noise level.

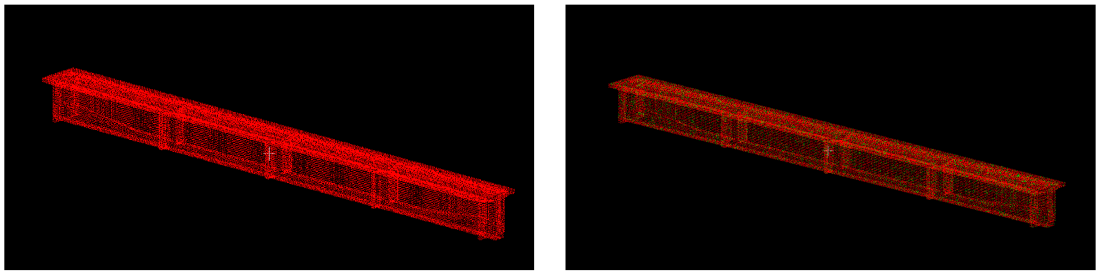
As shown in Table 7, both methods have relatively short runtimes at low noise levels. Their runtimes gradually increase with increasing noise levels, reaching a maximum at 6 mm, and then generally decrease. In comparison, S-FPFH achieves shorter runtimes under all tested conditions, with an average reduction of 22.42%.

It is worth noting that S-FPFH uses more descriptor centers than R-FPFH. For example, at a noise level of 10 mm, R-FPFH and S-FPFH use 8 and 17 descriptor centers, respectively, with corresponding runtimes of 64.67 s and 48.61 s. This indicates that the runtime advantage of S-FPFH is not due to a reduction in the number of descriptors. Because total runtime depends on multiple stages, including feature extraction, feature description, and pose estimation, the current results do not allow us to determine each stage's contribution to the runtime difference.

Both methods are timed from the completion of identical point cloud preprocessing procedures to the generation of the coarse registration results. For R-FPFH, the measured runtime includes random feature point selection, FPFH feature description, and SAC-IA coarse registration. For S-FPFH, it includes planar, linear, and corner feature extraction,

FPFH feature description, and SAC-IA coarse registration. The computational costs of region growing, plane fitting, Hough transform-based line detection, and α-shape boundary reconstruction are included in the total runtime. However, the runtime of each stage is not measured separately. Therefore, Table 7 and Figure 10 present the total runtime required by each method to complete coarse registration under identical preprocessing conditions.

To visually illustrate the point cloud alignment after coarse registration, we select one simulation result set for visualisation, as shown in Figure 11. Figure 11a shows the simulated point cloud generated from the BIM model of a standard 30 m precast T-girder. Figure 11b shows the overlaid source and target point clouds after coarse registration using S-FPFH. The main girder contours and major structural components exhibit good spatial continuity after registration. This indicates that the estimated initial pose enables effective alignment of the point clouds in this simulation case.



(**a**) (**b**)

Figure 11. Simulated precast T-girder point cloud and coarse registration result. (**a**) Simulated point cloud generated from the BIM model. (**b**) Superimposed source and target point clouds after coarse registration using S-FPFH.

4.3. Registration Experiments on Measured Point Clouds

Field data were acquired using a Trimble X7 terrestrial laser scanner (Trimble Inc., Westminster, CO, USA). Four consecutive scans were conducted on a single standard 30 m precast T-girder at a precast girder yard, as shown in Figure 12. The scanner has a nominal ranging accuracy of 2 mm. Under the selected scanning settings, the point spacings are 2.6 mm at 5 m, 18.0 mm at 35 m, and 41.2 mm at 80 m. Due to limited scanning space and line-of-sight conditions at the site, the scanner was positioned approximately 3 m from the girder. Multi-view point clouds of the girder were acquired from different scan stations.



Figure 12. T-girder data acquisition in a precast girder yard.

In the field experiments, R-FPFH is used as the baseline method. Both methods use the same FPFH descriptor and SAC-IA coarse registration framework, and ICP is applied to both methods for fine registration. The registration performance of the two descriptor center selection strategies is then compared using the field point cloud data.

The planar, linear, and corner features are extracted from the point clouds of each scan station using the same identification criteria. The visualization results are shown in Figure 13. These features are mainly distributed across the girder's main planar surfaces, structural boundaries, and geometric transitions, showing good correspondence with the geometric characteristics of the precast T-girder. Coarse registration is then performed between adjacent point clouds in scan-station order, followed by ICP fine registration using the coarse registration results as the initial poses. The same feature extraction thresholds and registration parameters are used for all scan stations.

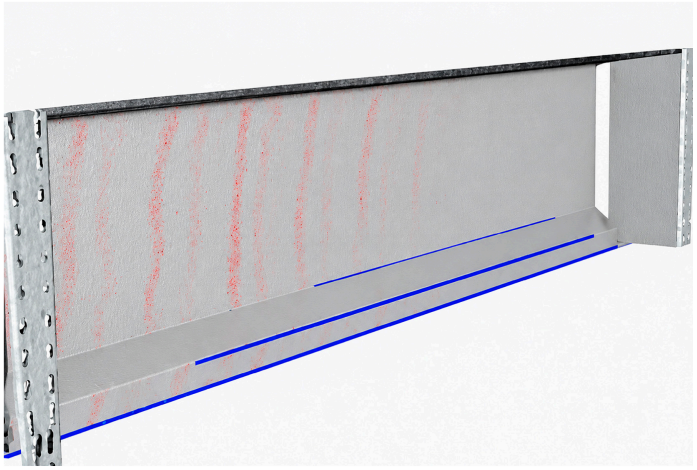
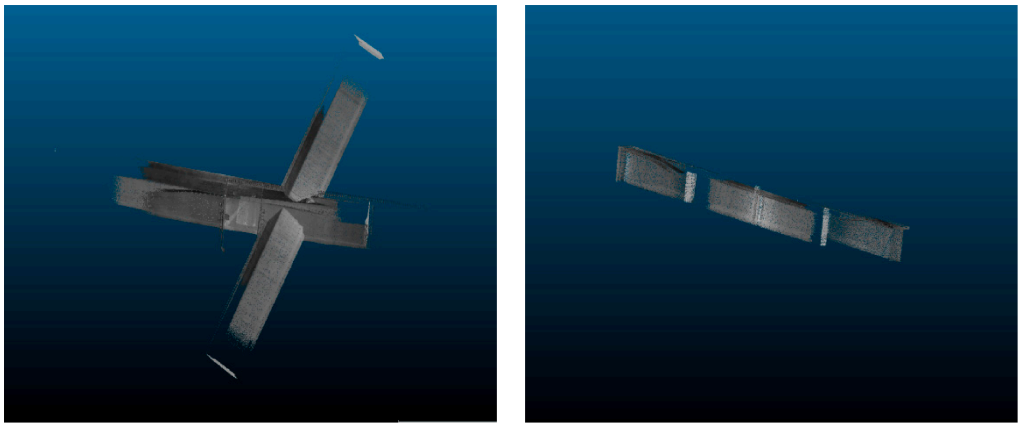


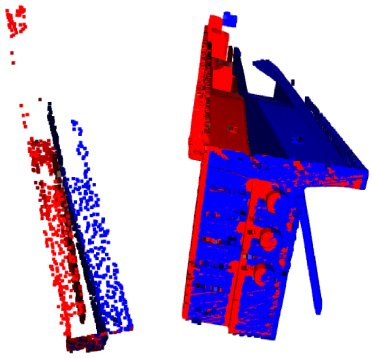
Figure 13. Structured feature extraction from measured T-girder point clouds. Blue lines represent the extracted linear features, while red points represent the planar features.

To visually compare the coarse registration results of the two methods, the point clouds from the first and second scan stations are selected as examples. The coarse registration results obtained using R-FPFH and S-FPFH are presented in Figures 14 and 15, respectively.



(**a**) (**b**)

Figure 14. Coarse registration results of measured T-girder point clouds from scan stations 1 and 2 using R-FPFH (visualized in CloudCompare version 2.13.2). (**a**) Overall point cloud misalignment. (**b**) Pronounced misalignment at the junction between the web and flange slab.



(**a**) (**b**)

Figure 15. Coarse registration results of measured T-girder point clouds from scan stations 1 and 2 using S-FPFH (visualized in the experimental environment). The red and blue point clouds represent the measured point clouds from scan stations 1 and 2, respectively. (**a**) Feature extraction and matching between the measured point clouds from two scan stations. (**b**) Registration result of the measured T-girder point clouds from two scan stations.

As shown in Figures 14 and 15, for this set of measured data, some misalignment remains in the overall girder contour and at the web-flange slab junction after coarse registration using R-FPFH. When structured feature points are used as FPFH descriptor centers, the major geometric boundaries of the two point clouds exhibit better alignment.

To compare the registration performance of the two methods, 10 repeated registration runs are performed on the same set of point clouds acquired from four scan stations. The average results for the three pairs of adjacent scan stations are presented in Table 8. These experiments evaluate algorithmic repeatability using a fixed point cloud dataset rather than independent field measurements.

Table 8. Comparison of measured registration results between the two methods over 10 repeated runs.

Performance Metric	R-FPFH	S-FPFH	Reduction (%)
Average Coarse Registration RMSE (mm)	14.29	5.37	62.42%
Average Coarse Registration Runtime (s)	128.20	92.30	28.00%
Average Fine Registration RMSE (mm)	11.14	2.12	80.97%
Average Total Registration Runtime (s)	710.10	490.00	31.00%

Note: The RMSE values in Table 8 represent the geometric alignment residuals between point clouds acquired from adjacent scan stations after registration. Since the field data lack an independent ground-truth pose reference, these values do not represent absolute registration errors relative to the ground-truth poses.

It should be noted that the coarse and fine registration RMSE values in Table 8 are calculated using the initial transformation estimated by SAC-IA and the final transformation refined by ICP, respectively. In both cases, RMSE is calculated as the root mean square of the distances between valid nearest-neighbor point correspondences after registration.

As shown in Table 8, compared with R-FPFH, S-FPFH reduces the average coarse registration RMSE from 14.29 mm to 5.37 mm, a 62.42% reduction. The average coarse registration runtime decreases from 128.20 s to 92.30 s, a reduction of 28.00%. After ICP fine registration, the average RMSE decreases from 11.14 mm to 2.12 mm, a reduction of 80.97%. The average total runtime of the registration process is reduced by 31.00%. These results indicate that S-FPFH achieves lower registration residuals and shorter runtimes for the tested field dataset. It also provides favorable initial alignment for subsequent ICP fine registration.

It should be noted that Table 8 mainly presents the average registration performance of the two methods using a fixed field dataset. The available summary results are insufficient to evaluate the variability among individual runs or the statistical significance of the observed differences. They also do not allow the convergence behavior of individual runs to be determined.

The registration results of adjacent scan stations are then combined sequentially to obtain the overall alignment of the four point clouds, as shown in Figure 16. After merging, the main girder contours and major structural components exhibit relatively good spatial continuity. This indicates that the proposed method achieves favorable multi-station point cloud merging results for the tested field dataset.

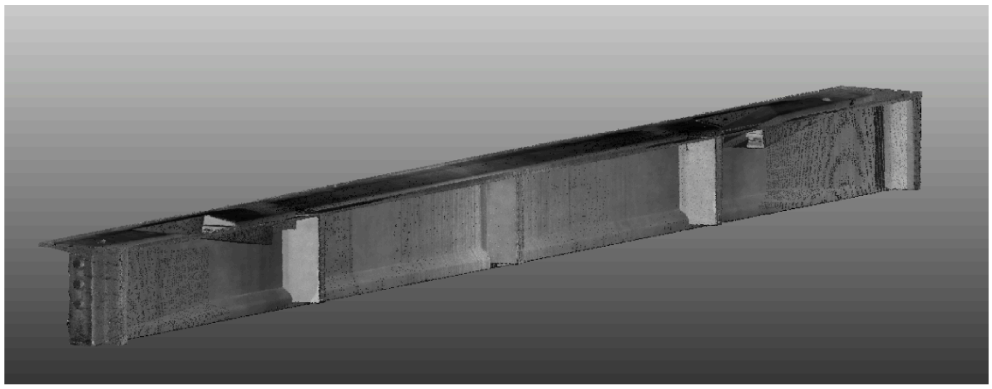


Figure 16. Final registration result of the four-station measured T-girder point clouds (visualized in CloudCompare).

5. Conclusions

This study proposes an FPFH-based coarse registration method guided by structured classification features to address the challenges of multi-station point cloud registration for precast T-girders in complex scanning environments at precast girder yards. The method is validated using simulated and field point cloud data. The main conclusions are as follows:

(1) To address the weak association between randomly sampled feature points and the main structural components of precast T-girders, engineering-oriented identification and extraction criteria for planar, linear, and corner features are established based on the regular geometry of precast T-girders. Representative points from these features are selected as FPFH descriptor centers. This allows structural prior information to guide descriptor center selection while retaining the standard FPFH descriptor and SAC-IA coarse registration framework.

(2) Simulation results show that S-FPFH achieves lower coarse registration residuals under most of the noise and local point cloud incompleteness conditions considered in this study. It also exhibits shorter runtimes in the noise experiments. However, fluctuations in registration performance are observed under certain noise conditions. This indicates that the registration performance of the proposed method remains dependent on the stability of the preceding structured feature extraction process.

(3) The registration results obtained from four scans of a single standard 30 m precast T-girder show that S-FPFH achieves lower coarse registration residuals and shorter runtimes than R-FPFH. It also provides favorable initial alignment for subsequent ICP fine registration and multi-station point cloud merging. The final merged point cloud exhibits good spatial continuity across the main structural components. These results provide preliminary evidence of the practical feasibility of the proposed method for the girder type and field scanning conditions examined in this study.

This study uses predefined geometric thresholds to extract structured features and adopts R-FPFH as the main baseline method. The current simulation experiments separately investigate the effects of Gaussian noise and local point cloud incompleteness. However, these two types of interference may occur simultaneously during actual scanning at precast girder yards. Future research will examine registration performance under severe loss of critical structural features and combined interference conditions. Different girder spans, cross-sectional geometries, and field scanning conditions will also be considered. In addition, we will introduce independent measurement references to validate the proposed method's applicability and improve the evaluation of registration accuracy.

Author Contributions: Conceptualization, Y.C.; methodology, Y.C.; software, Z.C.; validation, Z.C.; formal analysis, Y.C.; resources, H.Z.; data curation, Z.C.; writing—original draft, Z.C.; supervision, J.Z.; project administration, J.Z.; funding acquisition, H.Z. All authors have read and agreed to the published version of the manuscript.

Funding: This study was supported by the Ningbo Key Scientific and Technological Support Project in the Field of Transportation (Grant No. 2024032).

Data Availability Statement: The original contributions presented in this study are included in the article. Further inquiries can be directed to the corresponding author.

Conflicts of Interest: The authors declare no conflicts of interest.

References

1. Han, J.; Jang, M.; Han, H.; Shin, D.H. Automatic extraction of bridge dimensional information using 3D point cloud data. *KSCE J. Civ. Eng.* **2026**, *30*, 100312. [CrossRef]
2. Shu, J.; Zeng, Z.; Li, W.; Zhou, S.; Zhang, C.; Xu, C.; Zhang, H. Automatic geometric digital twin of box girder bridge using a laser-scanned point cloud. *Autom. Constr.* **2024**, *168*, 105781. [CrossRef]
3. Liu, D.; Chen, X.; Si, X.; Xia, R. Virtual assembly of large-scale bridge steel components based on supervoxels. *Appl. Laser* **2024**, *44*, 87–96. [CrossRef]
4. Hai, L.; Shulin, W.; Donghong, Z. Initial alignment for point cloud registration by improved differential evolution algorithm. *Optik* **2021**, *243*, 166856. [CrossRef]
5. Rusu, R.B.; Blodow, N.; Beetz, M. Fast Point Feature Histograms (FPFH) for 3D registration. In *Proceedings of the 2009 IEEE International Conference on Robotics and Automation, Kobe, Japan*; IEEE: New York, NY, USA, 2009; pp. 3212–3217. [CrossRef]
6. Li, Z.; Zhukun, L. Virtual Namesake Point Multi-Source Point Cloud Data Fusion Based on FPFH Feature Difference. *Sensors* **2021**, *21*, 5441. [CrossRef]
7. Liu, Y.; Zhang, Q.; Lin, S. An improved ICP point cloud registration algorithm based on fast point feature histograms. *Laser Optoelectron. Prog.* **2021**, *58*, 283–290. [CrossRef]
8. Jia, Z.; Liu, J.; Yang, H.; Huang, B.; Liu, H.; Ding, D. Adaptive FPFH registration incorporating dynamic downsampling. *Wuhan Univ. J. Nat. Sci.* **2026**, *31*, 217–224. [CrossRef]
9. Wang, Y.; Zhang, W.; Xie, L.; Chen, D. Point cloud registration algorithm using multi-scale feature fusion. *J. Northeast. Univ. Nat. Sci.* **2026**, *47*, 40–49. [CrossRef]
10. Jing, Y.; Lin, W.; Sheil, B.; Acikgoz, S. 3D multimodal feature for infrastructure anomaly detection. *Autom. Constr.* **2025**, *178*, 106388. [CrossRef]
11. Zhao, W.; Zhu, J.; Zhang, D.; Zhou, D. An Efficient Point Cloud Registration and Stitching Method Based on the FPFH Descriptor. *J. Anhui Univ. Technol. Nat. Sci.* **2024**, *41*, 627–635. [CrossRef]
12. Su, Z.; Zhou, G.; Tang, H.; Yuan, Y.; Liao, J.; Yu, W.; Lu, X.; Lv, L. Research on Point Cloud Registration Based on Key Points and Matching Point Pairs Algorithm. In *Proceedings of the IGARSS 2024-2024 IEEE International Geoscience and Remote Sensing Symposium*; IEEE: New York, NY, USA, 2024; pp. 10035–10038. [CrossRef]
13. Yang, L.; Xu, S.; Yang, Z.; He, J.; Gong, L.; Wang, W.; Li, Y.; Wang, L.; Chen, Z. Fast Registration Algorithm for Laser Point Cloud Based on 3D-SIFT Features. *Sensors* **2025**, *25*, 628. [CrossRef]
14. Yang, C.; Zhao, X.; Li, X.; Yu, Q.; Wei, H.; Jiang, Y.; Zheng, Z. PCSS: 3D Keypoint Detection for Point Clouds Using Structural Saliency. *IEEE Trans. Image Process.* **2025**, *34*, 2765–2780. [CrossRef]
15. Li, C.; Duan, Y. A Principal Direction-Guided Local Voxelisation Structural Feature Approach for Point Cloud Registration. *IET Comput. Vis.* **2025**, *19*, e70000. [CrossRef]

16. Slimani, K.; Tamadazte, B.; Achard, C. LoGDesc: Local Geometric Features Aggregation for Robust Point Cloud Registration. In *Proceedings of the Asian Conference on Computer Vision*; CVF: New York, NY, USA, 2024; pp. 1952–1968. Available online: https://openaccess.thecvf.com/content/ACCV2024/html/Slimani_LoGDesc_Local_geometric_features_aggregation_for_robust_point_cloud_registration_ACCV_2024_paper.html (accessed on 24 October 2026).
17. Liu, Y.; Wang, Z.; Huang, J.; Zhang, L. Robust Point Cloud Registration for Aircraft Engine Pipeline Systems. *Sensors* **2024**, *24*, 3358. [CrossRef]
18. Shan, Y.; Li, W.; Yang, M.; Ding, J.; Zhao, Y.; Tian, A. A Novel Pipeline Based on Line-Structured Features and Cross-Camera Perspectives for Coarse Aggregate Point Cloud Registration. *Expert Syst. Appl.* **2025**, *263*, 125761. [CrossRef]
19. Chen, R.; Yang, J.; Xiao, R.; Hui, Y.; Xu, A.; He, Q.; Xue, Z.; Guo, P. Scanned Point Cloud Registration for Localization of Aircraft Access Panel and Complementary Frame with Weak Features. *Adv. Eng. Inform.* **2025**, *65*, 103209. [CrossRef]
20. Zhao, T.; Li, L.; Tian, T.; Ma, J.; Tian, J. Patch-Guided Point Matching for Point Cloud Registration with Low Overlap. *Pattern Recognit.* **2023**, *144*, 109876. [CrossRef]
21. Gao, J.; Wang, P.; Dong, Q.; Zeng, Q.; Xin, S.; Zhang, C. D3Former: Jointly Learning Repeatable Dense Detectors and Feature-Enhanced Descriptors via Saliency-Guided Transformer. *Comput. Aided Geom. Des.* **2024**, *111*, 102300. [CrossRef]
22. Guo, L.; Chen, Z.; Cheng, S.; Yang, F.; Tao, W. Learning Compact and Overlap-Biased Interactions for Point Cloud Registration. *Neurocomputing* **2024**, *598*, 127949. [CrossRef]
23. Xu, Z.; Gao, X.; Jiang, X.; Cheng, S.; Zhang, Q.; Li, W.; Gao, X. S2Reg: Structure-Semantics Collaborative Point Cloud Registration. *Pattern Recognit.* **2025**, *161*, 111290. [CrossRef]
24. Liu, Y.; Zou, J.; Zhao, Y.; He, Y.; Liu, W.; Wang, N. Heterogeneous point cloud registration algorithm based on building contour features. *Bull. Surv. Mapp.* **2026**, *3*, 32–37. [CrossRef]
25. Mao, Q.; Xia, M.; Li, Q.; Zhu, J.; Fan, T. Global registration method for multi-station point clouds based on bundle adjustment. *Acta Geod. Cartogr. Sin.* **2024**, *53*, 1663–1670.
26. Xiong, G.; Cui, N.; Liu, J.; Zeng, Y.; Chen, H.; Huang, C.; Xu, H. Template-Guided Hierarchical Multi-View Registration Framework of Unordered Bridge Terrestrial Laser Scanning Data. *Sensors* **2024**, *24*, 1394. [CrossRef]
27. Wang, M.; Yi, F.; Li, L.; Huang, C. Point cloud registration based on adaptive local neighborhood feature extraction and matching. *Infrared Laser Eng.* **2022**, *51*, 431–440. [CrossRef]
28. Arun, K.S.; Huang, T.S.; Blostein, S.D. Least-Squares Fitting of Two 3-D Point Sets. *Pattern Anal. Mach. Intell.* **1987**, *9*, 698–700. [CrossRef]
29. Boehler, W.; Vicent, M.B.; Marbs, A. Investigating laser scanner accuracy. *Int. Arch. Photogramm. Remote Sens. Spat. Inf. Sci.* **2003**, *34*, 696–701.
30. Hu, Y.; Fang, X.; Zeng, W. Nonlinear least-squares solutions to the TLS multi-station registration adjustment problem. *ISPRS J. Photogramm. Remote Sens.* **2024**, *218*, 220–231. [CrossRef]
31. Lian, Z.; Wang, X.; Lin, J.; Zhang, L.; Tang, M. Second-order Spatial Measures Low Overlap Rate Point Cloud Registration Algorithm Based On FPFH Features. *AI Commun.* **2024**, *37*, 599–617. [CrossRef]

Disclaimer/Publisher's Note: The statements, opinions and data contained in all publications are solely those of the individual author(s) and contributor(s) and not of MDPI and/or the editor(s). MDPI and/or the editor(s) disclaim responsibility for any injury to people or property resulting from any ideas, methods, instructions or products referred to in the content.